PB88-218375

Numerical Simulation of Three-Dimensional Tuft Corona and Electrohydrodynamics

(U.S.) Environmental Protection Agency
Research Triangle Park, NC

1986

U.S. Department of Commerce
National Technical Information Service

TECHNICAL REPORT DATA
(Please read Instructions on the reverse before complet

1. REPORT NO.	2.	3.
EPA/600/J-86/464		PB88-218375

4. TITLE AND SUBTITLE	5. REPORT DATE
Numerical Simulation of Three-Dimensional Tuft Corona and Electrodynamics (Journal Version)	1986
	6. PERFORMING ORGANIZATION CODE
7. AUTHOR(S)	8. PERFORMING ORGANIZATION REPORT NO.
T. Yamamoto (RTI) and L. E. Sparks (EPA/AEERL)	
9. PERFORMING ORGANIZATION NAME AND ADDRESS	10. PROGRAM ELEMENT NO.
Research Triangle Institute P. O. Box 12194 Research Triangle Park, North Carolina 27709	11. CONTRACT/GRANT NO. CR810152-02
12. SPONSORING AGENCY NAME AND ADDRESS	13. TYPE OF REPORT AND PERIOD COVERED
EPA, Office of Research and Development **Air and Energy Engineering Research Laboratory** **Research Triangle Park, NC 27711**	Journal Article; June 1985 14. SPONSORING AGENCY CODE **EPA/600/13**

15. SUPPLEMENTARY NOTES AEERL project officer is Leslie E. Sparks, Mail Drop 54, 919/541-2458. Published in: IEEE Transactions on Industry Applications, Vol. 1A-22, No. 5, pp. 880-885.

16. ABSTRACT The paper discusses the numerical simulation of three-dimensional tuft corona and electrohydrodynamics (EHD). The importance of high-voltage and low-current operation in the wire-duct precipitator has focused attention on collecting high-resistivity dust. The local current density of individual tufts is considerably higher even at a low average current level and, therefore, could contribute to both the formation of back corona in the collected-dust layer and the generation of the secondary flow. Numerical simulation for three-dimensional tuft corona is successfully solved. The electrical characteristics of tuft corona are investigated, and the structure and role of the three-dimensional secondary flow and EHD in relation to transport of the fine particles are described.

17. KEY WORDS AND DOCUMENT ANALYSIS

a. DESCRIPTORS	b. IDENTIFIERS/OPEN ENDED TERMS	c. COSATI Field/Group
Pollution Dust Electrohydrodynamics Electric Corona Particles Electrostatic Precipitators Electrical Resistivity Mathematical Models	Pollution Control Stationary Sources Tuft Corona Numerical Simulation Particulate	13B 11G 20I 20C 14G 13I 12A

18. DISTRIBUTION STATEMENT	19. SECURITY CLASS (This Report)	21. NO. OF PAGES
Release to Public	**Unclassified**	8
	20. SECURITY CLASS (This page) **Unclassified**	22. PRICE

EPA Form 2220-1 (9-73)

REPRODUCED BY
U.S. DEPARTMENT OF COMMERCE
National Technical Information Service
SPRINGFIELD, VA. 22161

EPA/600/J-86/464
JOURNAL ARTICLE

Numerical Simulation of Three-Dimensional Tuft Corona and Electrohydrodynamics

TOSHIAKI YAMAMOTO AND LESLIE E. SPARKS

Abstract—**The importance of high-voltage and low-current operation in the wire-duct precipitator has focused attention on collecting high-resistivity dust. The local current density of individual tufts is considerably higher even at a low average current level and therefore could contribute to both the formation of back corona in the collected-dust layer and the generation of the secondary flow. Numerical simulation for three-dimensional tuft corona is successfully solved. The electrical characteristics of the tuft corona is investigated and the structure and role of the three-dimensional secondary flow and electrohydrodynamics in relation to transport of the fine particles is described.**

Introduction

HIGH-VOLTAGE and low-current operation in the wire-duct precipitator is an important issue that has drawn attention to the collection of high-resistivity dust [1]. Although it is well known that negative corona occurs as discrete tufts, existing analytical techniques for describing the negative corona have ignored the effects of the tufts that occur randomly and are often unstable on the corona wire. The tuft discharge in the negative corona, distinguished from uniform glow corona, is known to produce a strongly uneven current-density distribution with regions of very high current density immediately under each individual tuft discharge [2], [3]. This result could contribute to the formation of back corona in the collected-dust layer as well as the generation of the secondary flow.

A complete description of tuft corona and a fundamental understanding of the particle transport in the nonuniform electric field and fluid field are needed. It is necessary to establish a reasonably accurate physical model of the tuft corona. As an initial investigation, to take into account the field variations along the wire, numerical simulations were performed to investigate the characteristics of three-dimensional tuft corona. The results of numerical simulations allow us to describe the structure and role of the three-dimensional secondary flow and electrohydrodynamics in relation to transport of the fine particles. The particle sneakage caused by the secondary flow, known as electrical sneakage, is discussed in the sections that follow.

Paper IUSD 85-81, approved by the Electrostatic Processes Committee of the IEEE Industry Applications Society for presentation at the 1985 Industry Applications Society Annual Meeting, Toronto, ON, Canada, October 6-11. This work was supported by the US Environmental Protection Agency under cooperative agreement CR-810152-02. Manuscript released for publication March 17, 1986.

T. Yamamoto is with the Center for Aerosol Technology, Research Triangle Institute, P.O. Box 12194, Research Triangle Park, NC 27709.

L. E. Sparks is with the Air and Energy Engineering Research Laboratory, US Environmental Protection Agency, MD-61, Research Triangle Park, NC 27711.

IEEE Log Number 8609875.

Fundamental Equations for Three-Dimensional Tuft Corona

Maxwell and current-continuity equations are used to describe the electric field and current-density distributions. Under the assumptions of steady state and no effects of magnetic field, the governing equations for the electric field and space-charge-density distribution can be written as

$$\text{div grad } V = -\rho/\epsilon_o \tag{1}$$

$$\rho^2 = \epsilon_o \text{ grad } \rho \cdot \text{grad } V \tag{2}$$

$$\vec{E} = -\text{grad } V \tag{3}$$

$$\vec{J} = \rho(b\vec{E} + \vec{u}_f) \cong \rho b\vec{E} \tag{4}$$

where

- V voltage,
- $\vec{E}$ electric field,
- $\vec{J}$ current density,
- $\vec{u}_f$ fluid velocity,
- ϵ_o dielectric constant of air,
- ρ ionic space-charge density,
- b ion mobility.

Since the ion velocity is two orders of magnitude faster than the fluid velocity, $b\vec{E} \gg \vec{u}_f$, (4) can be decoupled from the fluid velocity.

Mathematical modeling of the tuft corona is initiated from Cooperman's analytical solutions [4]:

$$V(x, y) = V_o \frac{\sum_{m=-\infty}^{\infty} \ln \left\{ \frac{\cosh [\pi(x - 2mS_x)/2d] - \cos (\pi y/2d)}{\cosh [\pi(x - 2mS_x)/2d] + \cos (\pi y/2d)} \right\}}{\sum_{m=-\infty}^{\infty} \ln \left\{ \frac{\cosh (\pi m S_x/d) - \cos (\pi a/2d)}{\cosh (\pi m S_x/d) + \cos (\pi a/2d)} \right\}} \tag{5}$$

where

- V_o applied voltage,
- a radius of electrode,
- d wire-to-plate distance,
- m integer,
- S_x half distance between wires.

© 1986 IEEE
NTIS is authorized to reproduce and sell this report. Permission for further reproduction must be obtained from the copyright owner.

Fig. 1 describes the working domain in the wire-plate precipitator. A series of inner grid points for the numerical simulation of the given differential equations and the coordinates (x, y, z) are indicated in this figure; the origin of these coordinates is selected at the tuft on the wire. The finite difference approximation using the successive-over-relaxation method (SOR) becomes

$$V^{(l)}(i, j, k) = \frac{\omega}{2(1+\alpha^2+\beta^2)} \cdot \left\{ V^{(l-1)}(i+1, j, k) + V^{(l)}(i-1, j, k) + [V^{(l-1)}(i, j+1, k) + V^{(l)}(i, j-1, k)]\alpha^2 + [V^{(l-1)}(i, j, k+1) + V^{(l)}(i, j, k-1)]\beta^2 + \frac{\rho^{(l)}(i, j, k)}{\epsilon_o} h_x^2 \right\} + (1-\omega) V^{(l-1)}(i, j, k) \tag{6}$$

where $\alpha = h_x/h_y$, $\beta = h_x/h_z$, ω = extrapolation factor, and superscript (l) denotes the updated values.

Analogously, the finite difference approximation for the current continuity (2) becomes

$$\rho^{(l)}(i, j, k) = \frac{1}{2}(-\gamma + \sqrt{\gamma^2 + \delta^2}) \tag{7}$$

where

$$\gamma = \frac{\epsilon_o}{h_x}[E_x^{(l)}(i, j, k) + \alpha E_y^{(l)}(i, j, k) + \beta E_z^{(l)}(i, j, k)],$$

$$\delta = \frac{\epsilon_o}{h_x}[E_x^{(l)}(i, j, k)\rho^{(l)}(i-1, j, k) + \alpha E_y^{(l)}(i, j, k)\rho^{(l)}(i, j-1, k) + \beta E_z^{(l)}(i, j, k)\rho^{(l)}(i, j, k-1)]. \tag{8}$$

The solutions to (6) and (7) are obtained subject to the following boundary conditions.

- V V_o (applied voltage) along wire.
- J Known or measured average current density at plate.
- V 0 on ground plate (BCGF).
- E_x 0 on planes (ABFE) and (DCGH) except along wire (AE).
- E_y 0 on plane (AEHD) except along wire (AE).
- E_z 0 on planes (ABCD) and (EFGH).

Description of the Numerical Calculation Method

The numerical calculation method uses the charge-free and two-dimensional electrostatic potential distribution for the wire-duct geometry, given by (5), with a value of $m = 2$ because the value of $m > 2$ does not affect the potential distribution for this geometrical configuration. This potential expression is differentiated to give initial values of E_x and E_y as a function of position. The value of E_z is initially assumed to be zero. With these initial values and the desired current density, an initial estimate of space-charge density near the tuft can be obtained from (4). The tufts are assumed to be stationary and considered to be the only source of negative ions along the smooth wire without regard to the details of corona generation. Hence the detailed potential distribution near the electrode is beyond the scope of this study.

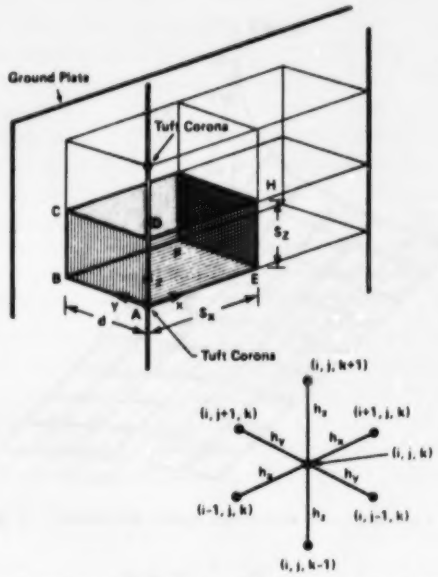

Fig. 1. Working domain and inner grid points in wire-duct precipitator.

The space-charge densities on lines (AB), (AE), and (AD) are first determined; for instance, the space-charge densities along line (AB) can be obtained by sweeping j in the increasing order since E_x and E_z in (8) are zero along line (AB). Their distributions on planes (ABFE), (ABCD), and (AEHD) are then calculated and, finally, on the entire volume domain (ABCDEFGH) is calculated by (7) using the initial values for the electric fields. Next the voltage is recomputed from (6) using the values of space-charge density just obtained. This procedure is repeated until the difference between the new and previous voltages at each point becomes within 0.001; i.e., convergence occurs. The voltage distribution is obtained by the superposition of Cooperman's analytical solution and the Poisson solution obtained by this iterative process. It should be noted that the most up-to-date values of $V^{(l)}$ are used for an iteration procedure. The best convergence rate was obtained for the value of $\omega = 1.70$.

The current density obtained by (4) is compared with the measured current density. If the computed and measured densities do not agree within 0.1 percent, the space charge near the tuft is re-evaluated by using all new values of E_y and ρ, and the process starts again. The same procedures are repeated alternately until agreement is achieved.

The numerical scheme of (6) was stable as long as the local field has a positive value and the cubical grid does not have an odd shape. The one-sided rather than space-centered difference in (8), at which the space-charge density was evaluated, has a first-order truncational error. Care must be taken to

select the grid size because it directly affects the space-charge density and the field distribution.

Numerical Results and Discussion

Electrical Characteristics of Tuft Corona

It has been found in separately published experimental work [2], [3] that the tuft onset voltage V_t was well below the Peek onset value V_c($V_t = 0.6V_c$). When the voltage is raised to the Peek onset value, the tufts become reasonably uniformly distributed along the full length of the wire. The voltage of $V_o = 42\,000$ V and measured current density of $J = 65\ \mu$A/m/plate were used for the numerical computation just above the value of V_c. The corresponding half-tuft spacing for a given voltage and geometry becomes $S_z = 2d/3$ (see [3] for the detailed tuft spacing versus voltage relationships). The other variables involved were standard temperature and pressure; $d = 0.114$ m, $a = 0.16$ cm, $S_x = 1.5d$, and $b = 2.0 \times 10^{-4}$ m^2/V/s. The grid points used for this computation were ($10 \times 7 \times 5$). The maximum error was within 7.0 percent when the grid points were doubled.

Fig. 2 presents the voltage ($\bar{V}$) distribution in the x-y plane at $z = 0$, normalized by the applied voltage V_o. The voltage due to the ionic space charge is relatively small since the current density is not large. The voltage distribution decreases slowly in the z-direction and approaches the charge-free analytical solution at $z = 2d/3$.

Fig. 3 shows the electric field in the y-component ($\overline{E_y}$) distribution in the x-y plane at $z = 0$ normalized by the average field $E_o = V_o/d$. The magnitude of $\overline{E_y}$ near the wire increases with the distance away from the tuft because the space-charge density decreases in the z-direction. On the other hand the $\overline{E_y}$ near the plate slowly decreases in the z-direction. The $\overline{E_y}$ distribution in general does not change greatly in the z-direction.

Fig. 4 shows the normalized field distribution in the x-component ($\overline{E_x}$) in the x-y plane at $z = 0$. The $\overline{E_x}$ near the wire increases in the z-direction from the tuft corona, but the $\overline{E_x}$ away from the corona wire decreases slowly in the z-direction.

Fig. 5 shows the normalized field distribution in the z-component ($\overline{E_z}$) in the x-y plane at $z = d/6$, where $\overline{E_z}$ distribution is at the maximum. The values of $\overline{E_z}$ are one order of magnitude smaller than those of $\overline{E_y}$ and $\overline{E_x}$, and the distribution of $\overline{E_z}$ decays slowly in the z-direction.

Fig. 6 presents the space-charge-density ($\bar{\rho}$) distribution in the x-y plane at $z = 0$, which is normalized by the value of space-charge density near the tuft (0.495×10^{-4} C/m^3). As can be seen from the figure, the maximum value occurs near the tuft and slowly decays in the x- and y-directions. The space-charge-density distribution sharply decreases in the z-direction and slowly increases in the y-direction, which is opposite to the direction shown in Fig. 6.

Fig. 7 shows the current-density ($\bar{J}$) distribution in the x-z plane, which is normalized by the maximum current density directly under the tuft. The current density decays sharply in the z-direction and extends in the x-direction due to the field contribution of the wire itself. As the wire radius increases,

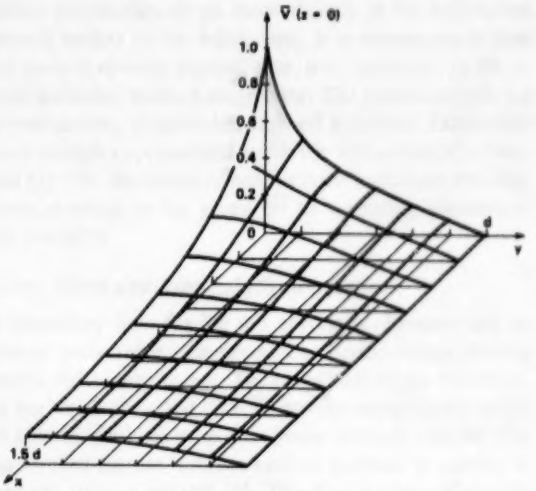

Fig. 2. Normalized voltage distribution in x-y plane at $z = 0$.

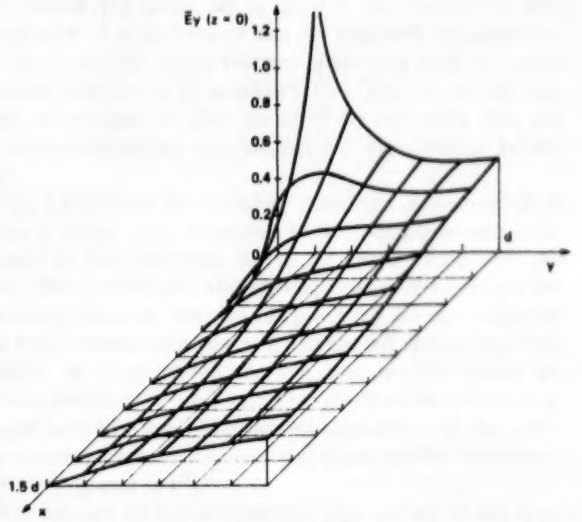

Fig. 3. Normalized field strength ($\bar{E}_y$) distribution in x-y plane at $z = 0$.

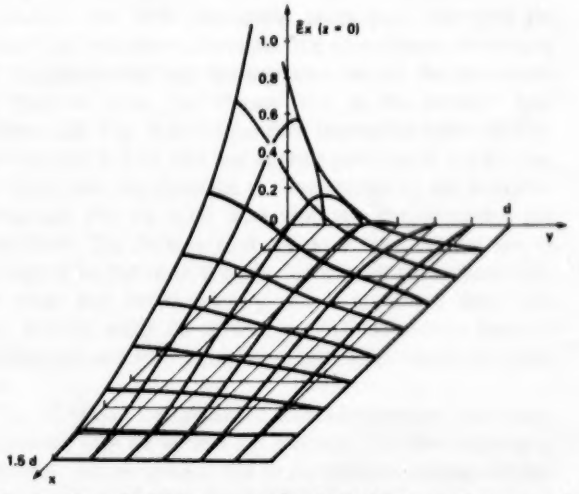

Fig. 4. Normalized field strength ($\bar{E}_x$) distribution in x-y plane at $z = 0$.

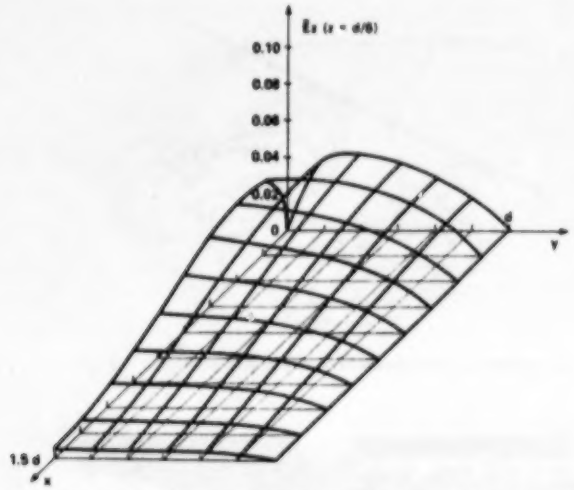

Fig. 5. Normalized field strength ($\bar{E}_z$) distribution in x-y plane at $z = d/6$.

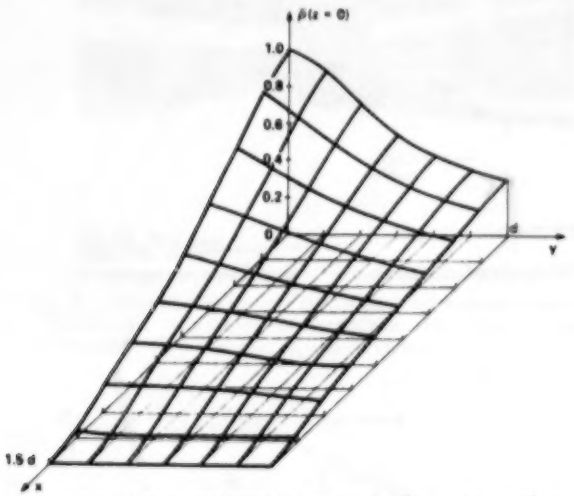

Fig. 6. Normalized space-charge-density ($\bar{\rho}$) distribution in x-y plane at $z = 0$.

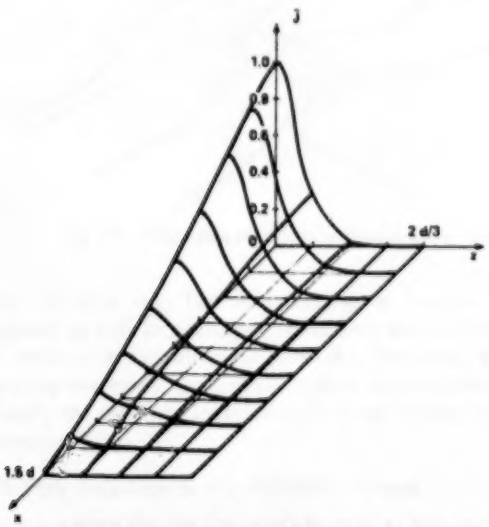

Fig. 7. Normalized current density ($\bar{J}$) distribution in x-z plane.

the current distribution drops more sharply in the z-direction and extends further in the x-direction. It is interesting to note that the current density beyond $z > d/3$ increases in the x-direction, although in small magnitude. The measurements for equicurrent density distribution showed a similar distribution [3]. Even though experimental work for tuft corona has been reported [2], [3], the measurement of current density distribution corresponding to the given set of operating parameters was not available.

Secondary Flow and Electrohydrodynamics

The secondary flow for the tuft corona is characterized by the electric body force: the product of space-charge density and electric field components. The magnitude of the secondary flow is not small since the current density immediately under the tuft corona is higher even with lower average current. The increase in total current is due to both an increase in number of tufts and the current per tuft [3]. The distributions of electric body force or current density with the flow visualization of the tuft corona [5] allow us to predict the secondary flow distribution. It is also shown that the rotational component of the current density causes vorticity production in the gas and is therefore the source of secondary flow [6]. An attempt was made to correlate the descriptions of the secondary flow and electrohydrodynamics with independent experimental knowledge.

Fig. 8 illustrates the secondary flow from individual tuft. It forms a vortex ring, elongated in the x-direction and compressed in the z-direction due to the electric field from the wire. Since individual tufts are different in strength and not stationary in nature, the vortices generated are less organized and more unstable between tufts. As the tuft spacing becomes smaller the rings merge together and smaller eddies are induced between the tufts, leading to the two-dimensional bell-shaped turbulent flow. The general dependence of the turbulent intensity on current density and mean gas-flow velocity is well summarized in [7].

For the case of two-dimensional glow corona in the wire-duct geometry, a pair of circulatory cells for the size of half-duct spacing are generated [8]. When the primary flow is introduced, the flow interaction takes place between the primary and secondary flows and the downstream circulatory cell disappears and only the upstream side of the circulatory cell remains under the corona wire as the primary flow increases [8]. Fig. 9 shows the flow interaction when primary flow velocity is 0.91 m/s and applied potential is 5.0 kV/cm. The white lines represent the gas streamlines by the Schlieren photograph and the solid lines represent the computed gas streamlines. The dark vertical region at the center is due to blockage from the vertical posts that support the corona wire. It is clear that the circulatory cell is generated above the plate, directly under the corona wire. Direct overlay between experimental and numerical streamlines show excellent agreement.

Fig. 10 shows the predicted three-dimensional electrohydrodynamic flow for various tuft spacings. The flow, starting at position a, moves upward due to the induced elliptic circulatory cell and is reflected down to the plate as it passes through

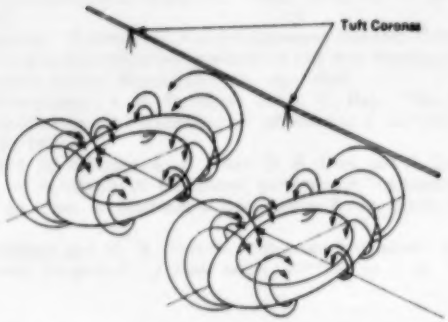

Fig. 8. Schematic diagram of three-dimensional secondary flow.

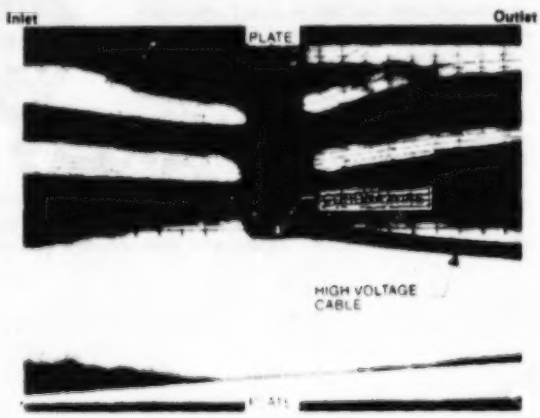

Fig. 9. Direct overlay between experimental and numerical streamlines. (White lines = experimental streamlines; solid lines = numerical streamlines. U_0 = 0.91 m/s; E_0 = 5.0 kV/cm.)

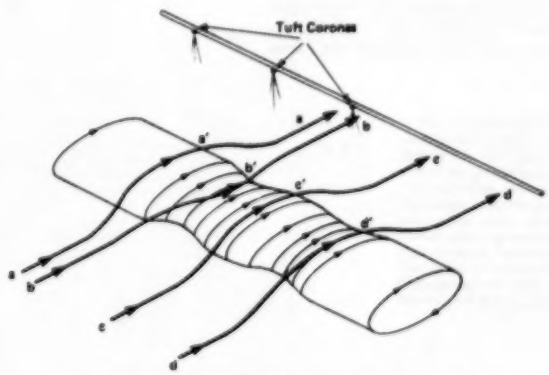

Fig. 10. Three-dimensional electrohydrodynamic field.

the cell (a-a′-a). The flow starting at position b moves upward as well as sideways (z-direction) because the cell size is reduced in this direction (b-b′-b). However, as the tuft spacing decreases, the upward motion increases everywhere. Finally the electrohydrodynamic field approaches two-dimensionality.

Particle Sneakage in the Negative Corona

It is known that the fine particles tend to follow closely the electrohydrodynamic streamlines. When the fine particles

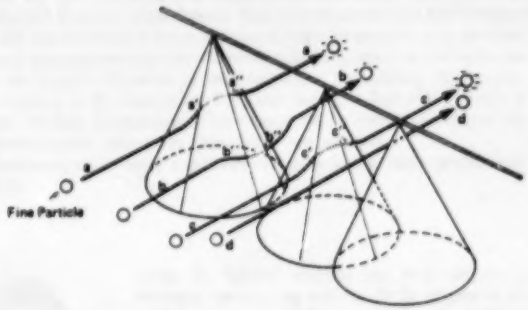

Fig. 11. Schematic diagram of electrical sneakage.

approach the tuft corona region, the particles tend to move between tufts due to the pressure generated by the corona discharge where the ionic-space charges are small. Therefore some particles sneak through the charging region as shown in Fig. 11. The particle starting at position a goes through the cone-shaped charging zone (a′-a″) and gets charged as shown in Fig. 11. The particle at b experiences a small charging time (b′-b″), which results in small charge on the particle. The particle at d completely sneaks through the charging zone and achieves no charge. This phenomenon is known as electrical sneakage and causes the reductions of charge on the particles and particle migration velocity, resulting in deleterious effects on the performance of the precipitator.

Conclusion

The mathematical model for the three-dimensional tuft corona was successfully developed. The results provide insight into the electrical characteristics, the secondary flow, and the electrohydrodynamic field for the negative tuft corona in a wire-duct precipitator. The major conclusions drawn from the present investigation are summarized as follows.

The secondary flow from the tuft corona forms a skewed vortex ring. When the tuft spacing becomes very small, the secondary flow becomes the two-dimensional bell-shaped turbulent flow. In the electrohydrodynamic field the elliptic secondary flow is generated directly under the corona wire, and as the tuft spacing decreases, the flow field becomes two-dimensional.

The fine particles tend to move between the tufts due to the secondary flow in which the electrical sneakage was realized, resulting in reduction of particle charging, particle migration, and collection efficiency.

References

[1] K. J. McLean, "Electrical characteristics of large diameter discharge electrodes in electrostatic precipitators," presented at the Fifth Symp. on the Transfer and Utilization of Particulate Control Technology, Kansas City, MO, Aug. 1984.

[2] P. A. Lawless, K. J. McLean, L. E. Sparks, and G. H. Ramsey, "Negative corona in wire-plate electrostatic precipitators: Part I. Characteristics of individual tuft-corona discharges," *J. Electrostatics*, vol. 18, pp. 199-217, 1986.

[3] K. J. McLean, P. A. Lawless, L. E. Sparks, and G. H. Ramsey, "Negative corona in wire-plate electrostatic precipitators: Part II. Calculation of electrical characteristics of contaminated discharge electrodes," *J. Electrostatics*, vol. 18, pp. 219-231, 1986.

[4] P. Cooperman, "A theory for space-charge limited currents with

application to electrical precipitation," *Trans. AIEE*, vol. 79, pp. 47-50, 1960.

[5] T. Yamamoto, "Investigation of three-dimensional secondary flow and the effects of particle transport," presented at 16th Ann. Meeting of the Fine Particle Society, Miami Beach, FL, Apr. 1985.

[6] E. J. Shaughnessy, J. H. Davidson, and J. C. Hay, "The fluid dynamics of electrostatic precipitators," submitted to *J. Aerosol Sci. Technol.*, 1985.

[7] S. A. Self, M. Mitchner, K. D. Khim, D. H. Choi, and R. Leach, "Effect of turbulence of precipitator performance," presented at Second Int. Conf. on Electrostatic Precipitation, Kyoto, Japan, Nov. 1984.

[8] T. Yamamoto and H. R. Velkoff, "Electrohydrodynamics in an electrostatic precipitator," *J. Fluid Mech.*, vol. 108, pp. 1-18, 1981.

Toshiaki Yamamoto received the B.S. and M.S. degrees in mechanical engineering from Sophia University, Tokyo, in 1967 and 1969, respectively. He received the M.S. degree in energy engineering from the University of Illinois, Chicago, in 1972 and the Ph.D. degree in mechanical engineering from Ohio State University, Columbus, in 1979.

He is a Research Engineer in the chemical engineering unit of Research Triangle Institute, Research Triangle Park, NC, where he is involved in modeling various aspects of electrostatic precipitator performance and electrostatic augmentation of fabric filtration. He has developed particle dynamics, concentration profiles, and efficiency theory in the electrohydrodynamic field, a narrow-gap corona model, tuft and point corona models, and related particle-sneakage theories. Before joining RTI, he was a Research Engineer at the Denver Research Institute at the University of Denver. He was involved in the evaluation of high-temperature high-pressure electrostatic precipitators and novel electrostatic precipitator technologies; he was also an Adjunct Professor in the Mechanical Engineering Department. Prior to working at the University of Denver, he was a Research Scientist at the United McGill Corporation, Columbus, OH, where he developed the electrohydrodynamic theories in electrostatic precipitators.

Dr. Yamamoto is currently a member of Sigma Xi and many professional associations.

Leslie E. Sparks received the M.S. degree in chemical engineering and the Ph.D. degree in air resources engineering from the University of Washington, Seattle.

He joined the US Environmental Protection Agency (EPA) in 1971, where he has managed projects to develop more efficient and cost-effective controls for particulate-matter emissions. His specialty has been advancing the state of the art in electrostatic precipitator (ESP) technology. He has recently managed development of low-cost multistage ESP's, an advanced computer model for ESP's—designed for use on personal computers—and the combined particulate and SO_x removal (E-SO_x) process.

Dr. Sparks is a member of the American Institute of Chemical Engineers, the American Association for the Advancement of Science, the Air Quality Coalition, and the Air Pollution Control Association. He is the author of numerous publications on control of particulate-matter emissions.

NOTICE

This document has been reviewed in accordance with U.S. Environmental Protection Agency policy and approved for publication. Mention of trade names or commercial products does not constitute endorsement or recommendation for use.

This article documents research that was conducted under the auspices of the U.S. Environmental Protection Agency (USEPA). As an arm of the government, the USEPA has a paid up, non-exclusive, irrevocable, worldwide license to reproduce, prepare derivative works, and distribute to the public all of the material contained herein, and to grant others acting on its behalf the right to do so. The USEPA grants to the National Technical Information Service, Department of Commerce, the right to act as its agent in the distribution of this material.